Characterisation of the Charge Collection Properties in a Segmented Planar HPGe Detector

E. Rintoul, A.J. Boston, H.C. Boston, A. Caffrey, J.R. Cresswell, L.J. Harkness-Brennan, D.S. Judson, P.J. Nolan, J. Platt, C. Unsworth, T.F. Woodroof

Oliver Lodge Laboratory, University of Liverpool, Liverpool, L69 7ZE, UK

I.H. Lazarus, J. Simpson

STFC Daresbury Laboratory, Daresbury, Warrington, WA4 4AD, UK

J. Cocks, D. Walker

Mirion Technologies (Canberra UK), Harwell, OX11 0RL, UK

B. Pirard, P. Quirin

Mirion Technologies (Canberra), Lingolsheim Facility, 67380 Lingolsheim, France

---

Abstract

Segmented germanium semiconductor detectors provide excellent γ-ray spectroscopic information whilst also being sensitive to the position of interactions within their active volume. Understanding the detector response to γ-ray interactions throughout its volume is required for interpreting the signal output. This work is the first assessment of the response and charge collection properties of an electrically-cooled Mirion Technologies-manufactured planar HPGe detector with boron implanted p^+ and amorphous germanium based n^+ strip contacts. The signal response of the detector as a function of γ-ray interaction position has been characterised by performing collimated beam scans with 59.5 keV and 661.7 keV γ-rays. A database of average signals, generated through the detector volume and across the detector surfaces, has been produced. A map of parameterised rise time response through depth has been generated and used to apply pulse shape analysis techniques, improving the position resolution within the detector.

Preprint submitted to Nuclear Instruments and Methods in Physics Research Section A October 6, 2021

Keywords: HPGe detector, Detector characterisation, Charge Collection, Pulse shape analysis

1. Introduction

This work reports on the characterisation of an electrically-cooled segmented germanium planar detector, manufactured by Mirion Technologies. The detector is part of a transportable γ-ray camera, which has been designed for locating and assaying radioisotopes in complex nuclear decommissioning environments. The cart-mounted system is comprised of two electrically-cooled planar position-sensitive semiconductor detectors which deliver excellent spectroscopic capabilities and allow for the reconstruction of γ-ray origins through Compton imaging [1]. The first layer is a Lithium-drifted Silicon (Si(Li)) detector [2] and the second a High-Purity Germanium (HPGe) detector.

The image quality of a Compton camera system is dependent upon the energy resolution and position resolution achievable within the detectors. For this reason, characterisation work has been carried out on the planar HPGe detector in order to quantify the experimental performance and to map the detector signal response as a function of γ-ray interaction position. This is necessary for the development and implementation of Pulse Shape Analysis (PSA) [3] algorithms to provide sub-voxel position resolution. Characterisation processes have been previously carried out at the University of Liverpool [4], [5] and, notably for this work, on the SmartPET HPGe detectors [6]. The detectors are geometrically similar to the detector studied in this work, and were manufactured with implanted $\sim$0.3 μm thick boron p^+ contacts and 180 μm thick lithium n^+ contacts [7]. The HPGe detector investigated within this work was produced with segmented contacts less than 1 μm thick. The n^+ contacts are based on amorphous germanium (a-Ge) while the p^+ are boron implanted. This is the first assessment and characterisation of a Mirion Technologies-manufactured planar detector that makes use of both this contact technology and electrical cooling techniques.

Parametric PSA methods applied to planar detectors can improve the position resolution in (x, y, z), defined in Figure 1, to potentially $1\times1\times1$ mm^3 [3] but cannot process multi-interaction events. These methods are typically light-weight and require low computational overheads. Quantification of image charge magnitudes induced in strips neighbouring the one collecting charge improves the lateral x or y position resolution for a given strip orientation. Characterisation of the charge pulse response throughout the detector's z-depth is required to improve the position resolution in this axis and has been carried out in this work. The time interval between collection of 10% and 30% of the total charge, T30 = t30 - t10, and the time between 10% and 90%, T90 = t90 - t10, can be used for rise time parameterisation in planar detectors [8].

2. Detector Specifications

The HPGe detector studied in this work is planar with an active volume of $60\times60\times20$ mm^3 surrounded by a 7.5 mm guard ring. A schematic diagram of the detector is shown in Fig. 1. Each 60×60 mm^2 face is segmented into 12 strips with horizontal AC p^+ and vertical n^+ DC coupled contacts; each with a pitch of 5 mm. Inter-strip gaps of 300 μm and 250 μm separate the AC and DC strips respectively, resulting in 144 position-sensitive voxels of $\sim5\times5\times20$ mm^3. Each strip is coupled with a warm Field Effect Transistor (FET) configuration charge-sensitive PSC823C preamplifier with a gain of 200 mV/MeV. The e^- collecting DC strips are grounded and an operational voltage of -1800 V, 500 V above depletion, is applied to the h^+ collecting AC strips. The detector is cooled using a Cryo-Pulse 5 Plus electrically powered cryostat that makes use of pulse tube cooling technology.

3. Detector Performance

An initial assessment of the detector was performed to record the energy resolution of each of the 24 strips at 122.1 keV with a 0.51 MBq ^{57}Co point source. The source was placed 12 cm from the DC side of the cryostat and

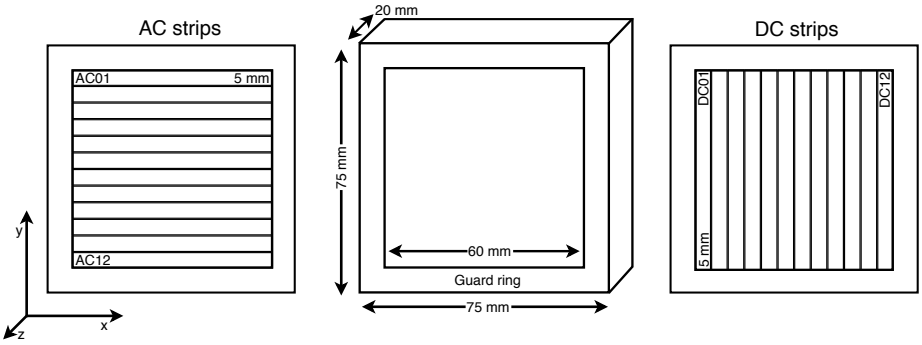

Figure 1: Schematic diagram of the HPGe detector crystal.

the preamplifiers sequentially output into a Canberra Model 2026 spectroscopy amplifier with a 4 μs Gaussian shaping time. An Ortec stand-alone 8k channel EASY-MCA was used to record this data and the Full Width at Half Maximum (FWHM) of the 122.1 keV photopeak was measured for each strip. The FWHM measurements are displayed in Fig. 2 for the 12 AC and 12 DC strips. The averages of each face are also displayed and were found to be 1.84 keV for the AC face and 1.58 keV for the DC face. The degraded AC energy resolution is a result of the increased capacitance of the AC-coupled preamplifiers.

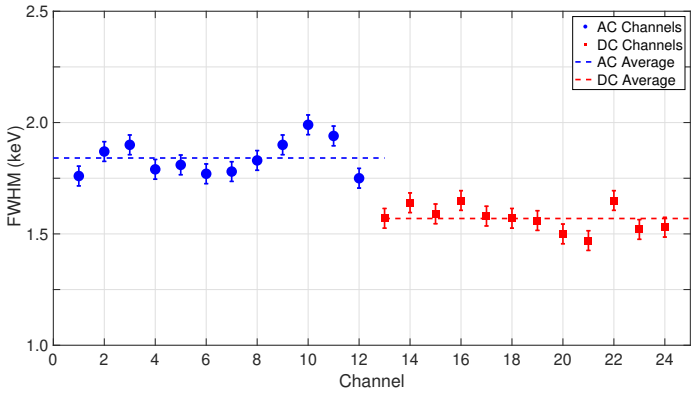

Figure 2: Analogue energy resolution of the 24 HPGe strips measured at 122.1 keV.

The electronic noise present in the system was measured as part of the detector performance assessment. The peak-to-peak noise of each strip was

measured with a MSO7104B Agilent oscilloscope at 1 MΩ impedance. The average peak-to-peak noise was calculated to be 2.9 mV for both the AC and the DC faces with little variation present. This compared well with geometrically similar HPGe detectors that made use of liquid nitrogen cooling as opposed to electrical cooling [9]. The detector has been calculated to have a 0.37% absolute efficiency at 661.7 keV, measured using a ^{137}Cs source placed 26.5 cm from the crystal.

4. Experimental Methodology

Collimated γ-ray scans were performed to characterise the detector signal response as a function of γ-ray interaction position, and to investigate the uniformity of the detector response. Surface scans were performed using low-energy γ-rays in order to investigate the response for interactions close to the AC and DC contacts as a function of x-y position and a side scan was carried out using high-energy γ-rays to characterise the response through z-depth.

The surface (x-y) scan utilised a 1 mm diameter, 40 mm length, tungsten collimator placed in a lead block containing a 1.64 GBq ^{241}Am source. This resulted in a maximum divergent beam spot size of 1.9 mm diameter incident on the front of the HPGe crystal. The collimated source was mounted on a Velmex motorised scanning system. This system gave full position control in x and y across the AC and DC detector faces. The source was moved in 1 mm steps with a precision of 100 μm across the faces of the detector and a dwell time of 10 s at each position. An incident count rate in the HPGe of ~450 59.5 keV γ-rays per second was recorded. The low penetration of ~1 mm from the ^{241}Am 59.5 keV γ-rays was used to produce surface scan maps. Scans were performed with the beam incident on each face of the detector to produce two surface maps.

A side (z-depth) scan was performed with a collimated 0.72 GBq ^{137}Cs source mounted atop a precision Parker scanning table [10], which enabled movement in x and z with an accuracy of 100 μm. The beam of 661.7 keV γ-rays produced

by the collimated ^{137}Cs source allowed penetration of the full crystal volume. A 180 mm long tungsten collimator with an internal diameter of 1 mm was used to collimate the isotropic source into a pencil beam. This resulted in a maximum beam spot diameter due to beam divergence of 1.8 mm incident on the base of the HPGe active crystal volume at $y = 0$ mm and 2.5 mm at $y = 60$ mm. The detector was mounted above the collimated γ-ray beam and the full 60×20 mm^2 side of the detector was scanned. The collimated source produced ~450 661.7 keV γ-rays per second and was moved in 1 mm steps with a dwell time of 300 s at each position.

The preamplifier outputs of the 24 strips were fed into a gain-offset box that applied a 5× gain and an offset to the signals. This allowed use of the full dynamic range of CAEN V1724 digitiser cards to which they were then input. The cards digitised the signals over a range of 2.25 V with 14-bit 100-MHz FADCs. A CAEN V1495 card was used to set trigger logic and ensure synchronised read-out, while a CAEN V2718 VME bridge card provided an optical link between the digitisers and a PCIe x8 CAEN Controller card mounted in a PC.

Digital Pulse Processing for Pulse Height Analysis (DPP-PHA) firmware within the V1724 cards was used to provide triggers after the application of a high-pass timing filter. Signals, 1.26 μs in length, from all channels were recorded if at least one AC and one DC channel registered a deposited energy greater than a trigger threshold of 8 keV. The leading edge of the charge collection pulses were centred in the signal length, such that the baseline and pulse height could be calculated. An inbuilt MWD-like trapezoidal filter with shaping parameters of 2.5 μs flat top and 7.5 μs rise time provided energy calculation through pulse height analysis. This set-up enabled the readout of all 24 detector channels along with calculated energies for every event. In this way the sum of energies deposited in all 12 strips across a face can be calculated to provide an "addback energy". Calculating the addback energy can recover the full energy following multiple interactions within the detector in which multiple strips on a given face register charge collection. Any strip

registering a DPP-PHA calculated energy of greater than a noise threshold of 5 keV, applied subsequent to the 8 keV event trigger threshold, was included in the summed addback for that face. This enabled inclusion of energies in the addback that fell below the trigger threshold.

5. Characterisation Results

5.1. ^{241}Am Surface Scan Results

Intensity maps showing the number of events with both AC and DC addback energies that passed a 56-62 keV photopeak gate as a function of collimator position are displayed in Fig. 3. Intensity maps are shown for a surface scan with the γ-beam incident on the AC contacts (a) and on the DC contacts (b). The AC strips are horizontal and are numbered 1-12 from top to bottom. The DC strips are numbered 1-12 from left-to-right and are vertical.

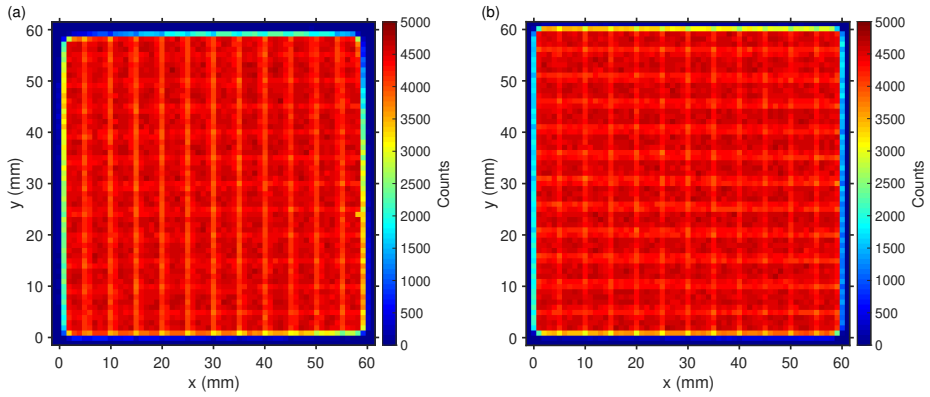

Figure 3: Intensity map from the AC surface scan (a) and the DC surface scan (b) for events that pass an addback energy gate around the ^{241}Am 59.5 keV photopeak.

The response was observed to be mostly uniform with a decrease in intensity occurring at x-y positions corresponding to inter-strip gaps. The reduction in intensity is attributed to a loss of charge occurring on the inter-strip gaps and was further investigated by reproducing the intensity plot with the added requirement of the interaction being single-pixel events and so confined to a $5\times5\times20$ mm^3 voxel. This is displayed in Fig. 4. The AC surface scan (a) shows

a decrease in counts for those inter-strip gaps that correspond to the vertical DC strips on the far-side relative to the incident γ-rays. The decrease is larger than that observed on the near-side horizontal AC inter-strip gaps. The larger reduction in counts for the DC surface scan (b) occurs between the AC strips which are on the far-side relative to the incident γ-rays.

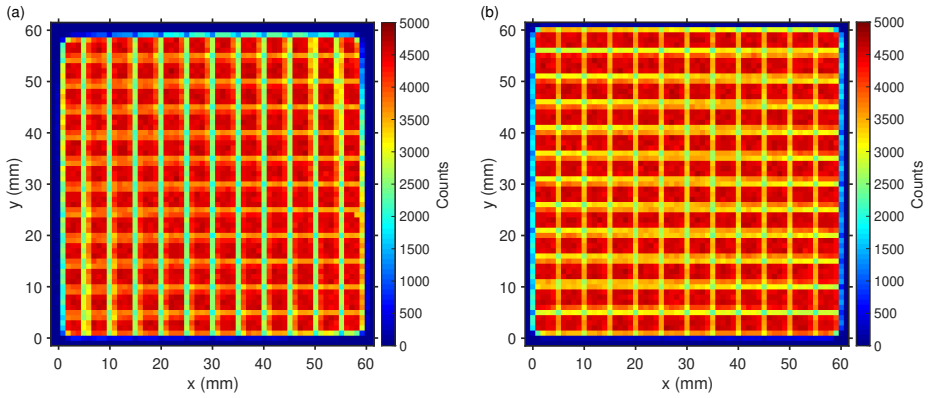

Figure 4: Intensity map from the AC surface scan (a) and the DC surface scan (b) for events that pass an addback energy gate and occur within a single pixel.

In germanium the cross section of Compton scattering is 6.7% that of photoelectric absorption [11] for 59.5 keV γ-rays. As such, it is assumed that the vast majority of interactions are photoelectric absorptions. The range of those γ-rays that do scatter is very small and so the probability of Compton scattering producing multi-strip events is low. For these reasons, the large drops in intensity at positions corresponding to the inter-strip gaps are not attributed to scattering, but instead to charge sharing events in which the collected charge is shared between two neighbouring strips. This is due to the splitting of lateral electric field lines [12] and results in exclusion of these events from the single-pixel maps in Fig. 4. As such, the charge shared varies in magnitude as a function of interaction position. In the cases of unequal charge sharing it is possible that some energy is lost due to the 5 keV low-energy noise threshold applied, resulting in the slight decreased observed in Fig. 3. These events are recovered by lowering the boundary on the photopeak energy gate.

Classification of this charge sharing effect is important as it potentially results in single interactions being recorded as multi-strip interaction events. In the Mirion-manufactured HPGe they were found to account for 12.3% of 59.5 keV γ-rays incident on the AC contacts and 11.9% of those incident on the DC contacts. This effect has been observed previously in germanium strip detectors [13], including in the previously mentioned SmartPET detectors [6].

In each case it is found that the larger percentage of charge shared events occur on the far-side strips relative to the incident γ-rays. This can be attributed to diffusion of the charge carrier cloud as it travels the full 20 mm z-depth of the detector to the far-side collecting strips [14]. As the charge sharing mechanism is a result of electric field line splitting between neighbouring strips, it is expected that the energy collected on each strip in a charge share event will vary as a function of the γ-ray interaction position.

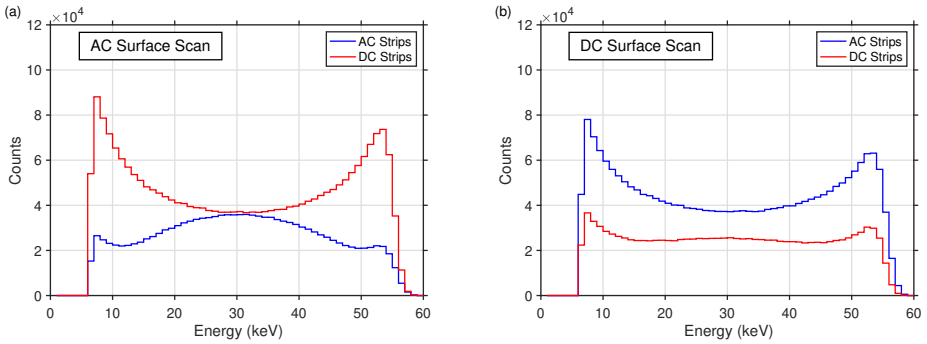

Figure 5: Energy spectra of events that occur in two neighbouring AC strips or two neighbouring DC strips for the AC surface scan (a) and DC surface scan (b). The total energy deposited in the two strips summed to 56-62 keV.

To investigate the charge shared through electric field splitting, spectra were produced for each surface scan for multi-strip events that occurred in either neighbouring AC or neighbouring DC strips. It was also required that each strip registered above 5 keV and the summed total passed the photopeak energy gate of 56-62 keV. The spectra are displayed in Fig. 5 for the AC surface scan (a) and the DC scan (b). In each case the predominance of charge share events can

be seen to occur on the far-face strips relative to the incident γ-rays. The AC surface scan shows a preference for equal charge sharing between the near-side AC strips with a maxima at 30 keV. Conversely the charge sharing between DC strips is more unequal with a minimum at 30 keV.

A similar result is observed for the DC scan but with less of a preference for equal sharing on the near-side DC strips. This is contrary to the results observed by Cooper *et al.* [7] in which strong electric field splitting caused unequal charge share between the AC strips when γ-rays were incident on the AC face. This was followed by more-equal charge share between the DC strips following drift of the charge carriers to the far-side strips. The inter-strip gap is of similar widths for the AC and DC strips so a disparity is not expected, though it may be a result of the a-Ge contact technology. In each case for the HPGe studied in this work the charge is equally shared on the near-side strips but at the far-side strips the carrier cloud is more strongly split.

The charge collection properties in the inter-strip gaps were studied further through the calculation of average charge collection times as a function of collimator position. T30 reveals information regarding the z-depth of interaction from the primary charge carriers for the collecting strip, and T90 is representative of the total charge collection time. The average T30 values were calculated from more than 1,500 single-voxel events that passed the photopeak gate and are displayed in Fig. 6 as rise time maps for AC T30 (a) and DC T30 (c) from the AC surface scan and AC T30 (b) and DC T30 (d) from the DC scan.

T30 times of $\sim$22 ns are observed for the charge collecting strips when the γ-rays are incident on the same face (a and d) while slower times of $\sim$75 ns are recorded when the charge carriers must travel the full 20 mm depth (b and c) to the collecting strips. A lack of uniformity is present in the charge collection times of strips on the same face and is attributed to the set-up of the preamplifiers. This is not expected to be a detector effect as each strip for a given face has the same capacitance.

Rise time differences are also observed along the length of the strips, with a decrease in T30 rise times occurring at the strip ends. Differences of up to

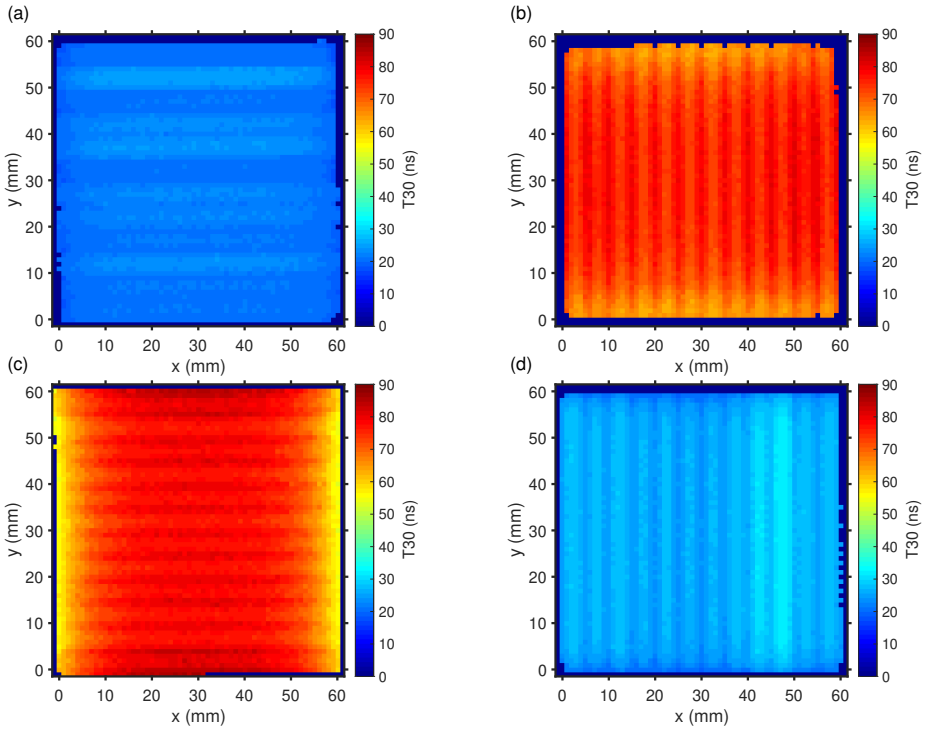

Figure 6: Average T30 rise time values produced as a function of collimator position for the AC surface scan AC collection (a) and the DC collection (b). The T30 rise times from the DC surface scan are displayed for the AC collection (c) and the DC collection (d).

30% are measured at the strip ends compared with the strip centre for AC charge collection for the DC scan (c). DC charge collection from the AC scan (b) has a smaller difference of 20% between the ends and centre. Both of these observations are contrary to previous observations of planar detectors in which a slightly weaker electric field at the detector edges was believed to yield longer rise times [2].

To investigate whether this variation was as a result of varying charge collection times or an artefact of parameterisation, average signals as a function of collimator position were formed. Each average was made of 200 single-pixel full-photopeak events, aligned to 50% of the total charge amplitude. Charge collection signals measured along the centre of AC06 when the γ-rays are incident

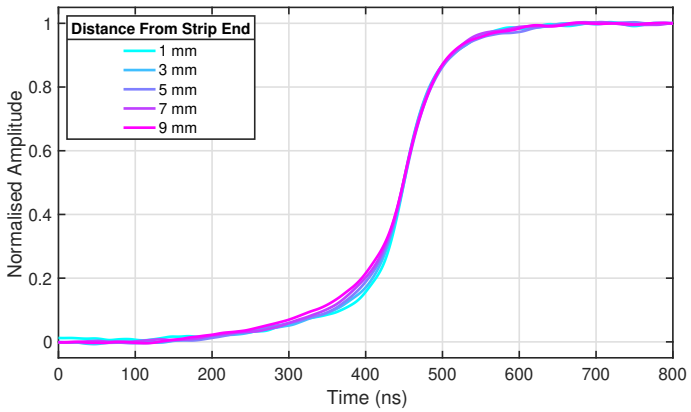

Figure 7: Average pulses corresponding to full photopeak, single-pixel events from AC06 for a selection of collimator distances from the strip end.

on the DC face are displayed in Fig. 7. The signals are taken from 1 mm to 9 mm away from the end of AC06 in 2 mm steps. The rise time variation is observed to be as a result of differences in the first ~30% of the signal shape. This part of the signal corresponds to the collection of primary charge carriers for a given face and indicates slower collection at the strip ends when the charge carriers must travel the bulk of the detector volume, though the total charge collection time remains the same. Variation of the rise times along the strips and on the inter-strip gaps are not seen when parameterisation is performed between 1% and 30%, t01-t30, or between 1% and 99%, t01-t99, of the collected charge. Parameterisation of the full signal length in this manner is only possible for averaged signals. It can be concluded that parameterisation of the charge collection pulse does not include all the information and can misrepresent the charge collection response of the detector. Rise time parameterisation PSA methods must so account for these signal variations across the detector faces.

Improvement of the position resolution in the lateral directions is performed through xy-PSA. Images charges induced in strips neighbouring that which is collecting charge are quantified by an asymmetry parameter, calculated using the method outlined by Cooper *et al.* [7]. The image charge response of the detector was investigated using the average signals produced when the 59.5 keV

γ-rays were incident on the AC contacts. Figure 8 shows the average charge collections signals and neighbouring image charges as the collimator was moved in 1 mm steps across the width of AC06 (top) and of DC06 (bottom).

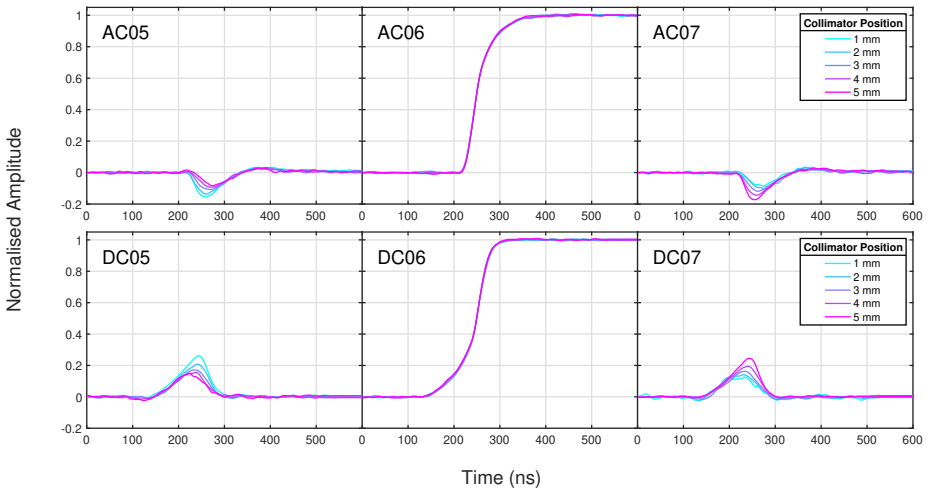

Figure 8: The average charge collection signal and neighbouring transient image charges for 5 collimator positions across the width of AC06 (top) and DC06 (bottom). produced from 59.5 keV γ-rays incident on the AC contacts.

The image charges were found to vary between 8% and 16% of the charge collection amplitude on the near-side AC strips, and between 14% and 26% on the far-side DC strips. The charge collection signal remained constant across the five positions. Asymmetry parameters found for these positions across the AC and DC strips are given in Table 1. Asymmetry parameters produced are found to change consistently across the 5 positions. Gates placed using these asymmetry parameters can be used to achieve position resolution x and y of up to 1 mm. The efficacy of this method is related to the deposited energy, as the larger the image charges produced the less the effect of noise on parameterisation of the area.

The varying signal shape along the strip lengths was found to produce smaller image charges at the strip ends compared to the strip mid-points. The image charges on each neighbouring strip changed in magnitude equally at each point

Collimator Position (mm)	1	2	3	4	5
AC Asym. Parameter	0.315	0.135	-0.073	-0.249	-0.390
DC Asym. Parameter	0.286	0.164	-0.084	-0.195	-0.376

Table 1: Parameterised asymmetry values obtained from average image charges neighbouring 59.5 keV interactions close to the AC contacts. Positions taken in 1 mm steps across the widths of strips AC06 and DC06.

along the strip and so the asymmetry parameterisation method used was found to be unaffected.

5.2. ^{137}Cs Side Scan Results

An intensity map of full photopeak ^{137}Cs events as a function of collimator position was produced from the side scan data. The map is displayed in Fig. 9 for addback energies that passed a photopeak energy gate of 657-665 keV. The DC strips are normal to the page numbered from left-to-right and are located at $z = 0$ mm while the AC strips, located at $z = 20$ mm, are parallel relative to the page and numbered 1-12 in increasing distance from the collimated source.

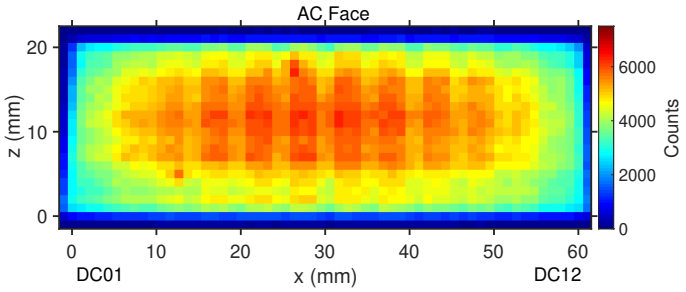

Figure 9: Photopeak gated ^{137}Cs addback events as a function of collimator position produced from the side scan with a gate of 657-665 keV (top).

The highest intensity of counts occurs centrally in the detector with the lowest around the edges. This distribution is expected due to the high probability of 661.7 keV γ-rays Compton scattering out of the crystal. γ-rays scattering near the edge of the active volume are more likely to be lost from the detector. A decrease in counts occurs in positions corresponding to the DC inter-strip gaps

and is attributed to the same charge loss mechanisms present in the surface scan. The side intensity profile shows little impact from any contact structure on the charge collection properties or attenuation from any crystal support.

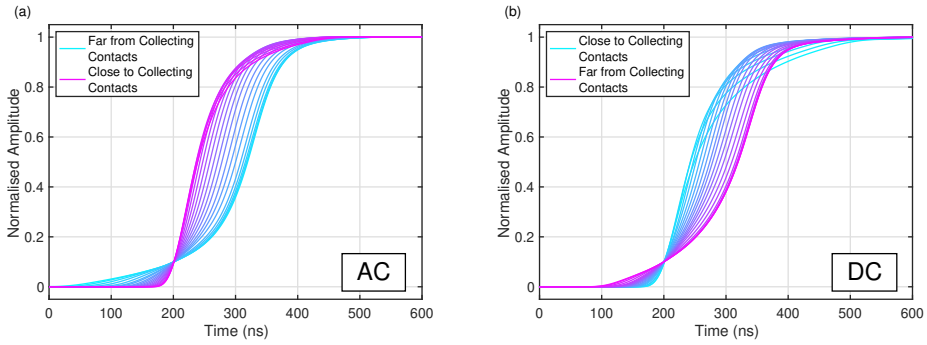

Figure 10: Average charge collection signals from each mm depth of the crystal which pass an RMS cut. Signals are aligned at t10.

To map the signal response through depth an average pulse was formed of 200 single-pixel full photopeak events for each strip at each z-depth. Events that scattered within a single-pixel were rejected through a root-mean-square (RMS) comparison of each individual signal to the average formed at that position. The average signals are displayed in Fig. 10 for strips AC06 (a) and DC06 (b) after alignment to 10% of the total charge collection (t10). The variation within the first 10% of the AC h^+ collection signal (a) is observed to be greater than that within the DC collection in the same range. Conversely the DC e^- collection has greater variation in the final 20% of the signal. In each case this is attributed to the slower mobility of the h^+ charge carriers [15].

The T30 and T90 signal rise times have been parameterised through the 20 mm z-depth of the detector and will be used to determine the γ-ray interaction position with z-PSA methods. The values have been plotted in 1 mm steps through the depth of the detector and are displayed in Fig. 11 for strips AC06 and DC06. The position is relative to the DC collecting strips. Error bars representing the standard error are too small to see.

The T30 response in Fig. 11a is mostly linear through the depth of the

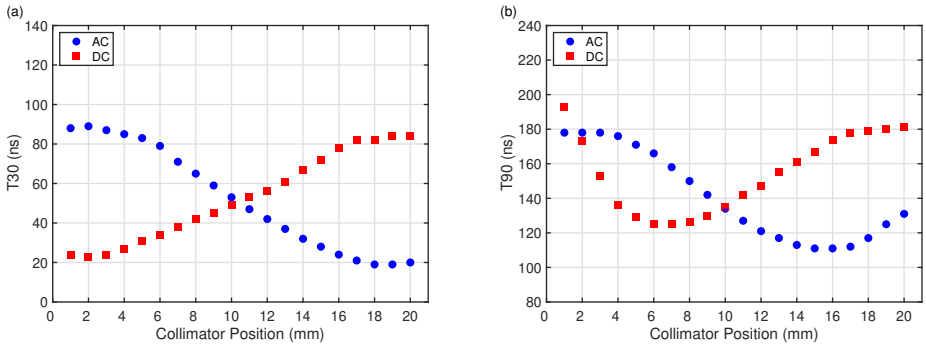

Figure 11: Parameterisation of pulses through depth produced for T30 and T90. The collimator mm position is relative to the DC charge collecting strips such that the DC contacts are located at 0 mm and the AC at 20 mm.

detector with a lack of sensitivity present close to the charge collecting strips. The linear component gives an indication of the sensitivity to position and was found to be 6 ns per mm for the AC T30 and 4 ns per mm for the DC T30. A characterisation of T50 was found to produce similar results. The T90 rise time distributions in Fig. 11b show a minima, corresponding to the fastest total charge collection time, located 5-6 mm away from each face of collecting strips. The T90 collection time increases at points that are close to collecting strips. As the detector is only 20 mm thick and the contacts 5 mm wide, the weighting field results in strips that are sensitive to charge collection throughout the entire z-depth. Hence, at these positions the total charge is not collected until the opposing charge carriers have been collected at the far face. Much of the T90 response is non-linear and so can not be easily quantified.

A method of parametric PSA for use in the planar HPGe detector was developed [16] that compared experimental T30, T50, and T90 values to an array of characterised values through a χ^2-minimisation. This method was tested with the parameterised rise time response values determined from the side scan for the AC and DC collection through depth. Separate rise time values were obtained for each pixel formed from the crossing of orthogonal AC and DC strips due to the variation in rise time response observed along detector

strips.

The detector was thus parameterised into 12×12×20 rise time pixels. Those events used in the formation of the average signals in Fig. 10 were then analysed with z-PSA. The difference between the collimator position in z, relative to the DC contacts, and the z-depth mm position determined with z-PSA were histogrammed. This is displayed in Fig. 12. As a percentage of total events, 48.3% were found at the same position as the collimator and 40.3% at ± 1 mm from it. In total 95.5% of events were found to be 2 mm or closer to the collimator position in z. Divergence of the collimated beam could account for many of the events being located 1-2 mm from the collimator position.

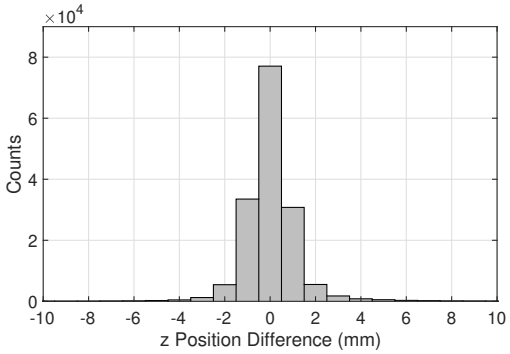

Figure 12: Difference in z-position found between collimator position of single-pixel, ^{137}Cs 661.7 keV signals and the z-position determined by parametric z-PSA.

The limitations of this method are attributed to the information lost through exclusion of the first and last 10% of the pulse in the parameterisation process. This information is typically hard to investigate in experimental pulses due to the presence of noise obfuscating the start and end points of the pulse. Parameterising the average charge collection signals allowed investigation of the t01-t30 and t01-t99 rise times of the total charge collection. These parameterisations are more representative of the time taken for the primary charge carriers for a given strip to be collected and the total time for all charge to be collected.

The information contained within the first 30% of the pulse reflects the position-sensitive nature of the primary charge carrier collection time for a given

strip; the first 10% of which is normally excluded. The parameterisation of t01-t30 is displayed in Fig. 13a. The relation observed is almost fully linear through the bulk of the detector with a sensitivity of 14 ns per mm for the AC collection and 7 ns per mm for the DC collection. Small change and low sensitivities only occur in regions close to the primary charge collecting strips but are more sensitive than those seen for T30.

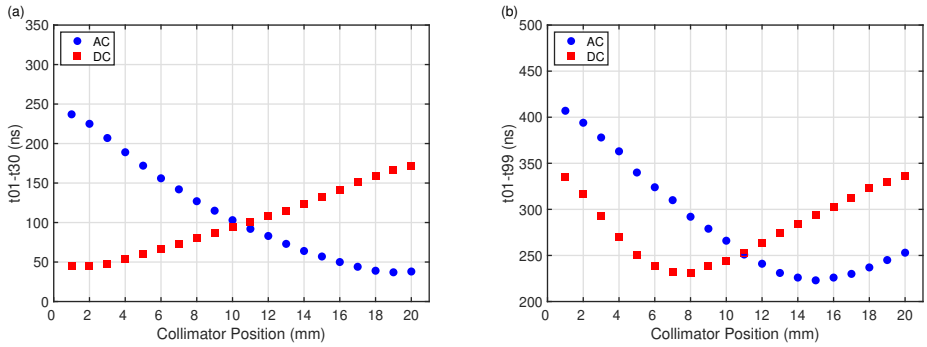

Figure 13: Parameterisation of the average AC06 and DC06 pulses through depth as t01-t30 (a) and t01-t99 (b), the time taken for the pulse to rise from 1% of the total height to 30% and 99% respectively.

The parameterisation profile through depth of t01-t99 is shown in Fig. 13b. The z-positions corresponding to the fastest charge collection and the equal charge collection times for each face are shifted relative to the T90 response observed in 11b. This shift represents a more accurate parameterisation of the charge collection properties of the detector when compared with T90 due to the differences in saturated drift velocities of the two carrier sets. Parameterisation between t01-t99 provides a linear response through all 20 mm z-positions when both AC and DC charge collection times are used. For the AC response this was found to be 16 ns per mm and 9 ns per mm for the DC response. This sensitivity is greater than that observed for T30 parameterisation and, unlike T90 parameterisation, provides high sensitivity near both sets of contacts.

6. Conclusion

This paper reports on the characterisation of an electrically-cooled, Mirion Technologies-manufactured planar HPGe that makes uses of a-Ge n^+ contacts. The average energy resolution has been found to be less than 1.9 keV and 1.6 keV for the AC and DC faces respectively at 122.1 keV. The noise presence in the detector has been quantified and the average peak-to-peak noise found to be < 3 mV for each face. These results compare well to geometrically-similar HPGe planar detectors constructed with different contact technology and without electrical cooling [6].

Collimated γ-ray scanning has been used to map the signal response across the detector x-y surfaces and through the z-depth. Charge sharing was quantified to be ~12% of surface events at 59.5 keV. Rise time maps of the surface charge collection properties have been produced and show a position dependence, a result of signal shape variation. Image charge asymmetry parameterisation has shown that a high degree of lateral position resolution of up to 1 mm can be achieved. A map of average signals through the 20 mm z-depth of the detector has been produced and the rise time response characterised as T30, T50, and T90. A linear sensitivity of 4 ns per mm and 7 ns per mm was found from T30 AC and DC respectively through the bulk of the detector. This allowed implementation of a χ^2-minimisation based PSA method to achieve sub-voxel position resolution in the HPGe z-depth which made use of all three rise time parameterisations. In total, 95.5% of 661.7 keV γ-ray interactions were found to be 2 mm or less in z-depth from a known collimator position. This represents a high position resolution through depth and enables effective use of the detector within the Compton camera cart system.

The limits of signal parameterisation have been investigated through parameterisation of the full length of averaged signals. This has shown how an increased sensitivity to position change of 16 ns per mm and 9 ns per mm for the AC and DC response respectively can be achieved as well as high sensitivity close to the contacts. To further improve system position resolution, and hence Compton camera imaging

performance, a simulated database of signals for the HPGe detector is currently being developed and will be validated using the average signals produced at constrained positions in this work. Signal database PSA methods utilise the full signal length for comparison unlike parametric based methods and can process multi-interaction events.

7. Acknowledgements

The authors would like to acknowledge funding contributions from STFC ST/N003543/1 and EPSRC EP/L015390/1.

References

References

[1] R. Todd, J. Nightingale, D. Everett, A proposed γ camera, Nature 251 (1974) 132–134.

[2] L. Harkness, D. Judson, A. Boston, H. Boston, J. Cresswell, P. Nolan, A. Sweeney, J. Beau, M. Lampert, B. Pirard, et al., Characterisation of a si(li) orthogonal-strip detector, Nuclear Instruments and Methods in Physics Research Section A: Accelerators, Spectrometers, Detectors and Associated Equipment 726 (2013) 52–59.

[3] K. Vetter, A. Kuhn, M. Deleplanque, I. Lee, F. Stephens, G. Schmid, D. Beckedahl, J. Blair, R. Clark, M. Cromaz, et al., Three-dimensional position sensitivity in two-dimensionally segmented hp-ge detectors, Nuclear Instruments and Methods in Physics Research Section A: Accelerators, Spectrometers, Detectors and Associated Equipment 452 (2000) 223–238.

[4] M. R. Dimmock, A. J. Boston, H. C. Boston, J. R. Cresswell, L. Nelson, P. J. Nolan, C. Unsworth, I. H. Lazarus, J. Simpson, Characterisation results from an agata prototype detector, IEEE Transactions on Nuclear Science 56 (2009) 1593–1599.

[5] C. Unsworth, A. Boston, H. Boston, L. Harkness-Brennan, D. Judson, P. Nolan, O. Thomas, J. Wright, A. Adekola, J. Colaresi, et al., Characterisation of a small electrode hpge detector, Nuclear Instruments and Methods in Physics Research Section A: Accelerators, Spectrometers, Detectors and Associated Equipment 927 (2019) 293–300.

[6] H. Boston, A. Boston, R. Cooper, J. Cresswell, A. Grint, A. Mather, P. Nolan, D. Scraggs, G. Turk, C. J. Hall, et al., Characterisation of the smartpet planar germanium detectors, Nuclear Instruments and Methods in Physics Research Section A: Accelerators, Spectrometers, Detectors and Associated Equipment 579 (2007) 104–107.

[7] R. Cooper, A. Boston, H. Boston, J. Cresswell, A. Grint, L. Harkness, P. Nolan, D. Oxley, D. Scraggs, I. Lazarus, et al., Charge collection performance of a segmented planar high-purity germanium detector, Nuclear Instruments and Methods in Physics Research Section A: Accelerators, Spectrometers, Detectors and Associated Equipment 595 (2008) 401–409.

[8] R. Cooper, A. Boston, H. Boston, J. Cresswell, A. Grint, A. Mather, P. Nolan, D. Scraggs, G. Turk, C. Hall, et al., Smartpet: Applying hpge and pulse shape analysis to small-animal pet, Nuclear Instruments and Methods in Physics Research Section A: Accelerators, Spectrometers, Detectors and Associated Equipment 579 (2007) 313–317.

[9] G. H. B. Turk, The characterisation of the first SmartPET HPGe planar detector, Ph.D. thesis, University of Liverpool, 2006.

[10] M. Descovich, Improving the position resolution of highly segmented HPGe detectors using pulse shape analysis methods, Ph.D. thesis, University Of Liverpool, 2002.

[11] M. Berger, J. Hubbell, S. Seltzer, J. Chang, J. Coursey, R. Sukumar, D. Zucker, K. Olsen, Xcom: Photon cross sections database, nist

standard reference database 8 (xgam), URL http://physics. nist. gov/PhysRefData/Xcom/Text/XCOM. html (2010).

[12] M. Amman, P. Luke, Three-dimensional position sensing and field shaping in orthogonal-strip germanium gamma-ray detectors, Nuclear Instruments and Methods in Physics Research Section A: Accelerators, Spectrometers, Detectors and Associated Equipment 452 (2000) 155–166.

[13] W. Coburn, S. Amrose, S. E. Boggs, R. P. Lin, M. S. Amman, M. T. Burks, E. L. Hull, P. N. Luke, N. W. Madden, 3d positioning germanium detectors for gamma-ray astronomy, in: X-Ray and Gamma-Ray Detectors and Applications IV, volume 4784, International Society for Optics and Photonics, 2003, pp. 54–64.

[14] R. Kroeger, N. Gehrels, W. Johnson, J. Kurfess, B. Phlips, J. Tueller, Charge spreading and position sensitivity in a segmented planar germanium detector, Nuclear Instruments and Methods in Physics Research Section A: Accelerators, Spectrometers, Detectors and Associated Equipment 422 (1999) 206–210.

[15] L. Mihailescu, W. Gast, R. Lieder, H. Brands, H. Jäger, The influence of anisotropic electron drift velocity on the signal shapes of closed-end hpge detectors, Nuclear Instruments and Methods in Physics Research Section A: Accelerators, Spectrometers, Detectors and Associated Equipment 447 (2000) 350–360.

[16] A. Caffrey, The development and evaluation of a Compton camera for imaging spent fuel rod assemblies, Ph.D. thesis, University of Liverpool, 2019.